Commun. Comput. Phys.
doi: 10.4208/cicp.030211.040811a

Vol. **12**, No. 3, pp. 767-788
September 2012

A High Order Spectral Volume Formulation for Solving Equations Containing Higher Spatial Derivative Terms II: Improving the Third Derivative Spatial Discretization Using the LDG2 Method

Ravi Kannan*

CFD Research Corporation, 215 Wynn Drive, Huntsville AL 35805, USA.

Received 3 February 2011; Accepted (in revised version) 4 August 2011

Available online 1 March 2012

Abstract. In this paper, the second in a series, we improve the discretization of the higher spatial derivative terms in a spectral volume (SV) context. The motivation for the above comes from [J. Sci. Comput., 46(2), 314–328], wherein the authors developed a variant of the LDG (Local Discontinuous Galerkin) flux discretization method. This variant (aptly named LDG2), not only displayed higher accuracy than the LDG approach, but also vastly reduced its unsymmetrical nature. In this paper, we adapt the LDG2 formulation for discretizing third derivative terms. A linear Fourier analysis was performed to compare the dispersion and the dissipation properties of the LDG2 and the LDG formulations. The results of the analysis showed that the LDG2 scheme (i) is stable for 2^{nd} and 3^{rd} orders and (ii) generates smaller dissipation and dispersion errors than the LDG formulation for all the orders. The 4^{th} order LDG2 scheme is however mildly unstable: as the real component of the principal eigen value briefly becomes positive. In order to circumvent the above, a weighted average of the LDG and the LDG2 fluxes was used as the final numerical flux. Even a weight of 1.5% for the LDG (i.e., 98.5% for the LDG2) was sufficient to make the scheme stable. This weighted scheme is still predominantly LDG2 and hence generated smaller dissipation and dispersion errors than the LDG formulation. Numerical experiments are performed to validate the analysis. In general, the numerical results are very promising and indicate that the approach has a great potential for higher dimension Korteweg-de Vries (KdV) type problems.

AMS subject classifications: 65

Key words: Spectral volume, LDG2, LDG, higher spatial derivative terms, KDV, Fourier analysis.

*Corresponding author. *Email address:* sunshekar@gmail.com (R. Kannan)

1 Introduction

We continue with the development of the spectral volume (SV) method for solving equations containing higher spatial derivative terms, following the first paper in the series [17], wherein a LDG flux discretization method was employed for handling equations containing third derivative terms. The ultimate goal of this research study is to have a spectral volume formulation for equations containing higher spatial derivative terms, with the following attributes: (a) high order accurate; (b) easily applicable to multi dimensional problems; (c) geometrically flexible; (d) easily hook up with an implicit solver and algebraic, geometric and polynomial multigrid preconditioners and (e) easily extendable (eventually) for even higher (fourth or more) spatial derivative terms.

The spectral volume method was originally formulated Wang et al. [25, 31–35] and further developed by Kannan et al. [12–22] for conservation laws on unstructured grids. The spectral volume method can be viewed as an extension of the Godunov method to higher order by adding more degrees-of-freedom (DOFs) in the form of sub cells in each cell (simplex). The simplex is referred to as a spectral volume (SV) and the subcells are referred to as control volumes (CV). All the SVs are partitioned in a geometrically similar manner in a simplex, and thus a single reconstruction is obtained. The DOFs are then updated to high-order accuracy using the usual Godunov method.

The SV method was successfully implemented for 2D Euler [34] and 3D Maxwell equations [25]. The quadrature free formulation was implemented by Harris et al. [9]. A *h-p* adaptation was also carried out in 2D [10]. Recently Sun et al. [29] implemented the SV method for the Navier Stokes equations using the LDG [7] approach to discretize the viscous fluxes. Kannan and Wang [14, 22] conducted some Fourier analysis for a variety of viscous flux formulations. Kannan implemented the SV method for the Navier Stokes equations using the LDG2 (which is an improvised variant of the LDG approach) [15] and DDG approaches [16]. Even more recently, Kannan extended the SV method to solve the moment models in semiconductor device simulations [12, 13]. A new high order boundary condition was developed in the SV context for inviscid flows by Kannan [18]. A SV formulation for the line contact Elastohydrodynamic Lubrication problem was developed by Kannan [19].

In this paper, we adapt the LDG2 formulation for solving equations containing third spatial derivative terms in a SV context. The LDG2 formulation was recently proposed by Kannan and Wang [15], as an improvement to the traditional LDG formulation. The LDG2 formulation is more symmetrical and displays higher accuracy than the LDG formulation. Fourier analysis was performed on the LDG and the new variant (LDG2) and these yielded some interesting results on accuracy and stability of the formulation. Numerical tests were performed to confirm the above.

The paper is organized as follows. In the next section, we review the basics of the SV method. The LDG formulation for high order spatial derivatives is presented in Section 3. A detailed linear analysis is performed for the LDG formulation in Section 4. Section 5 presents with the different test cases conducted in this study. Finally conclusions from

this study are summarized in Section 6.

2 Basics of the spectral volume method

2.1 Formulation in 1D

Consider the general conservation equation

$$\frac{\partial Q}{\partial t}+\frac{\partial(f_i(Q)-f_v(Q))}{\partial x}=0 \tag{2.1}$$

in a one dimensional domain Ω with appropriate initial and boundary conditions. In (2.1), x refers to the Cartesian coordinate and $(x)\in\Omega$, $t\in[0,T]$ denotes time, Q is the vector of conserved variables, and f_i and f_v are the inviscid and viscous fluxes respectively. Domain Ω is discretized into I non overlapping sub cells. In the SV method, the simplex grid cells are called SVs, denoted S_i, which are further partitioned into CVs, denoted C_{ij}, which depend on the degree of the polynomial reconstruction. Fig. 1 shows linear, quadratic and cubic partitions in 1D. The partitions were originally determined for a linear advection equation using a linear Fourier analysis [30]. One of the outcomes of this paper is to obtain stable and accurate partitions for equations having third derivatives.

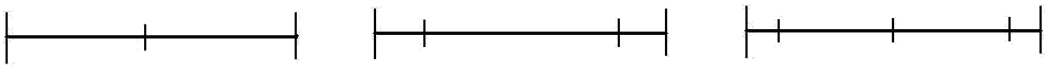

(a) (b) (c)

Figure 1: Partitions of a SV in 1D. Case (a): Linear reconstruction; Case (b): Quadratic reconstruction; Case (c): Cubic reconstruction.

We need N unknown control volume solution averages (or DOFs) to construct a degree k polynomial. N is calculated using the below formula (in 1D)

$$N=k+1, \tag{2.2}$$

where k is the degrees of the polynomial, constructed using the CV solution averages. The CV averaged conserved variable for C_{ij} is defined as

$$\overline{Q}_{i,j}=\frac{1}{V_{i,j}}\int_{C_{i,j}}QdV, \qquad j=1,\cdots,N, \quad i=1,\cdots,I, \tag{2.3}$$

where $V_{i,j}$ is the volume of C_{ij}. Given the CV averaged conserved variables, a degree k polynomial can be constructed such that it is $(k+1)^{\text{th}}$ order approximation to Q. In other words, we can write the polynomial as

$$p_i(x)=\sum_{j=1}^{N}L_j(x)\overline{Q}_{i,j}, \tag{2.4}$$

where the shape functions $L_j(x,y)$ satisfy

$$\frac{1}{V_{i,j}}\int_{C_{i,j}} L_n(x)dV=\delta_{j,n}, \tag{2.5}$$

where $\delta_{j,n}$ is the Kronecker delta. Eq. (2.1) is integrated over the C_{ij}. This results in the following equation

$$\frac{\partial\overline{Q}}{\partial t}+\frac{1}{V_{i,j}}\sum_{r=1}^{K}\int_{Ar}(\vec{F}\cdot\vec{n})dA=0, \tag{2.6}$$

where $\vec{F}=(f_i-f_v)$ where Ar represents the r^{th} face of C_{ij}, $\vec{n}$ is the outward unit normal vector of Ar and K is the number of faces in C_{ij} (two in 1D). The fluxes are discontinuous across the SV interfaces. The inviscid fluxes can be handled using a numerical Riemann flux, such as upwinding, the Rusanov flux [27], the Roe flux [26] or AUSM flux [24]. In this manuscript, upwinding is employed to handle the inviscid fluxes. The handling of the viscous fluxes is discussed below.

2.2 Spectral volume formulation for the diffusion equation

The following diffusion equation is considered first in domain Ω with appropriate initial and boundary conditions

$$\frac{\partial u}{\partial t}-\nabla\cdot(\mu\nabla u)=0, \tag{2.7}$$

where μ is a positive diffusion coefficient. We define an auxiliary variable

$$\vec{q}=\nabla u. \tag{2.8}$$

Eq. (2.7) then becomes

$$\frac{\partial u}{\partial t}-\nabla\cdot(\mu\vec{q})=0. \tag{2.9}$$

Using the Gauss-divergence theorem, we obtain

$$\overline{\vec{q}_{ij}}V_{ij}=\sum_{r=1}^{K}\int_{Ar}u\cdot\vec{n}dA, \tag{2.10a}$$

$$\frac{d\overline{u_{ij}}}{dt}V_{ij}-\sum_{r=1}^{K}\int_{Ar}\mu\vec{q}\cdot\vec{n}dA=0, \tag{2.10b}$$

where $\overline{\vec{q}_{ij}}$ and $\overline{u_{ij}}$ are the CV averaged gradient and solution in C_{ij}. As the solution u is cell-wise continuous, u and $\vec{q}$ at SV boundaries are replaced by numerical fluxes $\underline{\vec{q}}$ and $\underline{u}$.

The above equations thus become

$$\overrightarrow{\overline{q_{ij}}}V_{ij}=\sum_{r=1}^{K}\int_{Ar}\bar{u}\cdot\vec{n}dA, \tag{2.11a}$$

$$\frac{d\overline{u_{ij}}}{dt}V_{ij}-\sum_{r=1}^{K}\int\mu\vec{q}\cdot\vec{n}dA=0. \tag{2.11b}$$

The LDG formulation

The commonly used approach for obtaining the numerical fluxes is the LDG approach. In this approach, the numerical fluxes are defined by alternating the direction in the following manner [29]

$$\overline{u}=u_L, \tag{2.12a}$$

$$\overline{\vec{q}}=\vec{q}_R, \tag{2.12b}$$

where u_L is the left state solutions of the CV face in consideration and $\vec{q}_R$ is the right state solution gradients of the face (of the CV) in consideration. Thus if the CV face lies on the SV boundary, $u_L\neq u_R$ and $\vec{q}_L\neq\vec{q}_R$ (assuming that the function is not smooth).

The LDG2 formulation

The LDG2 can be explained using the following notations:

I. e_{CV} refers to the CV boundary.

II. e_{SV} refers to the SV boundary.

III. $e_{CV1}=e_{CV}\cap e_{SV}$ refers to the intersection of the CV and SV boundaries.

IV. $e_{CV2}=e_{CV}/e_{CV1}$ refers to the set theoretic complement of e_{CV} and e_{CV1} (i.e., set of all surfaces present in e_{CV} but not in e_{CV1}).

V. $u_A=(u_L+u_R)/2$ is the average of the left and right state solutions.

The crux of the LDG2 approach is maintaining two gradients for the residual computation:

I. The first gradient is the right-sided gradient ($\overrightarrow{qr}$). The CV averaged $\overrightarrow{qr}$ is computed using u_R.

II. The second gradient is the averaged gradient ($\overrightarrow{q\alpha}$). The CV averaged $\overrightarrow{q\alpha}$ is computed using u_A.

Thus for a given SV, the CV averaged values of $\overrightarrow{q\alpha}$ depend only on the CV averaged solution of the current SV and its closest neighbors. The CV averaged values of the $\overrightarrow{qr}$ depend only on the CV averaged solution of the current SV and the SV to its right. Given the above CV averages, reconstructions are performed to obtain $\overrightarrow{qr}_L$, $\overrightarrow{qr}_R$, $\overrightarrow{q\alpha}_L$, $\overrightarrow{q\alpha}_R$. $\overrightarrow{qr}_L$ is used for computing the viscous fluxes through the CV faces lying on e_{CV1}. Either $\overrightarrow{q\alpha}_L$ or $\overrightarrow{q\alpha}_R$ can be used for computing the viscous fluxes through the CV faces lying on e_{CV2}. This procedure ensures compactness.

3 SV for higher spatial derivatives

We will explain the procedure using a linear equation; consider the following simple linear equation with the appropriate initial and boundary conditions

$$u_t + u_{xxx} = 0. \tag{3.1}$$

Rewriting the above into a first order system yields:

$$u_t + p_x = 0, \quad p = q_x, \quad q = u_x. \tag{3.2}$$

Integrating (3.2) over the CV and application of Gauss-divergence theorem yields:

$$\frac{d\bar{u}_{ij}}{dt} V_{ij} + \sum_{r=1}^{K} \int_{Ar} \vec{p} \cdot \vec{n} dA = 0, \tag{3.3a}$$

$$\overline{\vec{p}_{ij}} V_{ij} = \sum_{r=1}^{K} \int_{Ar} q \cdot \vec{n} dA = 0, \tag{3.3b}$$

$$\overline{\vec{q}_{ij}} V_{ij} = \sum_{r=1}^{K} \int_{Ar} u \cdot \vec{n} dA = 0. \tag{3.3c}$$

u, p and q at SV boundaries are replaced by numerical fluxes $\underline{u}$, $\underline{\vec{p}}$ and $\underline{\vec{q}}$. Eqs. (3.3a), (3.3b) and (3.3c) can be solved by extending the LDG method discussed in [14, 15, 29] to higher derivatives (shown in the below subsection).

3.1 The LDG formulation

In this approach, the numerical fluxes are defined by alternating the direction of the numerical fluxes. There are two choices:

- Choice a

$$\underline{u} = u_L, \quad \underline{\vec{q}} = \vec{q}_R, \quad \underline{\vec{p}} = \vec{p}_R. \tag{3.4}$$

- Choice b

$$\underline{u} = u_R, \quad \underline{\vec{q}} = \vec{q}_R, \quad \underline{\vec{p}} = \vec{p}_L. \tag{3.5}$$

Though there are a total of eight choices (two for each variable), six of them are unconditionally unstable. More details can be found in [36, 37]. The size of the stencil is 5 (optimal).

3.2 The LDG2 formulation

Two numerical fluxes are used in this approach. The first numerical flux uses an alternating formulation. Either of the formulations given in Eq. (3.4) or Eq. (3.5) can be used as the alternating formulation. The second numerical flux is given by:

$$\underline{u}=u_R, \qquad \underline{\vec{q}}=\frac{(\vec{q_L}+\vec{q_R})}{2}, \qquad \underline{\vec{p}}=\vec{p}_L|\vec{p}_R. \tag{3.6}$$

The first numerical flux is used, when the CV boundary in consideration belongs to e_{CV1}. The second numerical flux is used, when the CV boundary in consideration belongs to e_{CV2}. The CV averaged value of $\vec{q}$ is computed using the right state values of u. A reconstruction is performed to obtain a high order accurate approximation of $\vec{q}$ at the CV boundaries. Two different formulations are used to obtain the CV averaged value of $\vec{p}$:

I. The first formulation uses the right state value of $\underline{\vec{q}}$. This corresponds to the first numerical flux. Let us denote this CV average as $\overline{\vec{p}}_1$.

II. The second formulation uses the average of the left and the right state values of $\underline{\vec{q}}$. This corresponds to the second numerical flux. Let us denote this CV average as $\overline{\vec{p}}_2$.

Reconstructions are performed to obtain high order accurate approximations for each of $\overline{\vec{p}}_1$ and $\overline{\vec{p}}_2$. The left state of $\vec{p}_1$ is used as the numerical flux, during the update of the solution u, when the CV boundary in consideration belongs to e_{CV1}. Either of the left or the right states of $\vec{p}_2$ can be used, during the update of the solution e_{CV2}, when the CV boundary in consideration belongs to e_{CV2}. It can be seen that the overhead in LDG2 comes from computing, storing and performing reconstructions for $\vec{p}$.

It can be seen that the size of the stencil is still 5. Moreover, the inherent asymmetry of the LDG scheme is drastically reduced, by employing a central formulation for $\underline{\vec{p}}$ for the CV boundaries belonging to e_{CV2}. The central formulation is also expected to increase the overall accuracy of the scheme (shown in later sections, using Fourier analysis and actual numerical experiments). The above attributes of the LDG2 hold good even in higher dimensions.

4 Fourier analysis for the new formulation

In this analysis, we follow a technique described by Zhang and Shu [38] and focus on linear, quadratic and cubic reconstructions. The SV is partitioned into two equal CVs for the second order simulations. The CVs for the third and the fourth order are clustered toward the SV boundaries. The locations of the CV faces (i.e., nodes in 1D) were based on the Gauss quadrature points. For the sake of simplicity, let us first consider a linear partition shown in Fig. 2. In this case, all the formulations can be cast in the following form:

$$\frac{d}{dt}\begin{bmatrix}\bar{u}_{j,1}\\ \bar{u}_{j,2}\end{bmatrix}=A\begin{bmatrix}\bar{u}_{j-2,1}\\ \bar{u}_{j-2,2}\end{bmatrix}+B\begin{bmatrix}\bar{u}_{j-1,1}\\ \bar{u}_{j-1,2}\end{bmatrix}+C\begin{bmatrix}\bar{u}_{j,1}\\ \bar{u}_{j,2}\end{bmatrix}+D\begin{bmatrix}\bar{u}_{j+1,1}\\ \bar{u}_{j+1,2}\end{bmatrix}+E\begin{bmatrix}\bar{u}_{j+2,1}\\ \bar{u}_{j+2,2}\end{bmatrix}, \tag{4.1}$$

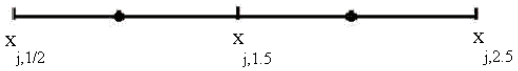

Figure 2: Linear spectral volume in 1D.

where A, B, C, D and E are constant matrices. We now seek a general solution of the following form

$$u(x,t)=\hat{u}_k(t)e^{ikx}, \tag{4.2}$$

where k is the index of modes $(k=1,2,\cdots)$ representing the wave number and $\hat{u}_k$ is the amplitude of the given wave. Obviously, the analytical solution for Eq. (3.1) is $u(x,t)=e^{i(kx+k^3t)}$. The solution we are looking for can be expressed as

$$\begin{bmatrix} \bar{u}_{j,1} \\ \bar{u}_{j,2} \end{bmatrix} = \begin{bmatrix} \hat{u}_{k,1} \\ \hat{u}_{k,2} \end{bmatrix} e^{ikx_{j,\frac{3}{2}}}. \tag{4.3}$$

Substituting Eq. (4.3) into Eq. (4.1), we obtain the advancement equation:

$$\begin{bmatrix} \hat{u}'_{k,1} \\ \hat{u}'_{k,2} \end{bmatrix} = G(k,h) \begin{bmatrix} \hat{u}_{k,1} \\ \hat{u}_{k,2} \end{bmatrix}, \tag{4.4}$$

where the amplification matrix is given by

$$G=e^{-2ikh}A+e^{-ikh}B+C+e^{ikh}D+e^{2ikh}E. \tag{4.5}$$

The above method can be easily extended to 3rd and 4th orders. In general, all but one of the eigen values of G is made up of spurious modes and is damped rapidly. This is under the assumption that the scheme is stable (ensured by making sure that the real part of the eigen values is non positive). The error associated with the scheme and the convergence properties can be determined by analyzing the non spurious mode. It must be noted that both discretization methods (Eq. (3.4) or Eq. (3.5)) will yield identical results during this analysis procedure.

4.1 Second order spatial analysis

Fig. 3 shows the variation of the real component of the principal eigen value with respect to the non dimensional frequency $\xi=kh$ for the second order SV. As expected all the values in Fig. 3 are non-positive for both the LDG and the LDG2 formulations. It can be seen that the LDG2 formulation has a smaller dissipation than the LDG formulation. Fig. 4 shows the deviation between the imaginary components of the principal (numerical) eigen value and the analytical eigen value (i.e., $i\xi^3$) as a function of ξ. It can be seen that the LDG2 formulation generates smaller dispersion errors than the LDG formulation.

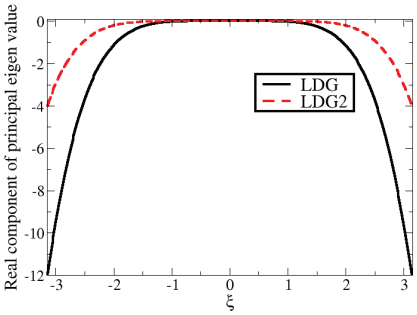

Figure 3: Plot of the real component of the principal eigen value as a function of the non-dimensional frequency for the second order SV.

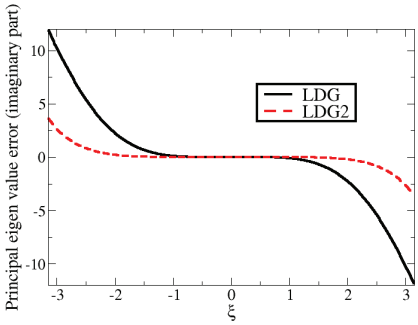

Figure 4: Plot of the error associated with the imaginary component of the principal eigen value as a function of the non-dimensional frequency for the second order SV.

4.2 Third order spatial analysis

The third order SV of unit length has its interior CV boundaries given by the following local coordinates: $\{0,d,1-d,1\}$, where d is the length of the first CV in the SV. A value of $d=0.1$ was deemed most accurate in the first paper of this series [17]. This will be used in the remainder of the paper. Fig. 5 shows the variation of the real component of the principal eigen value with respect to the non dimensional frequency ξ for the third order SV. As expected all the values in Fig. 5 are non-positive. Once again, the LDG2 formulation has a smaller dissipation than the LDG formulation. Similarly Fig. 6 shows the deviation between the imaginary components of the principal (numerical) eigen value and the analytical eigen value (i.e., $i\xi^3$) as a function of ξ. The LDG2 formulation generated smaller dispersion errors than the LDG formulation.

Even though the LDG2 outperforms the LDG formulation, it can be seen that the 2^{nd} order LDG2 formulation is more accurate than the 3^{rd} order LDG2 at large wave numbers. Similar trends were observed by Kannan and Wang during their analysis of the LDG2 viscous flux discretization formulation [15].

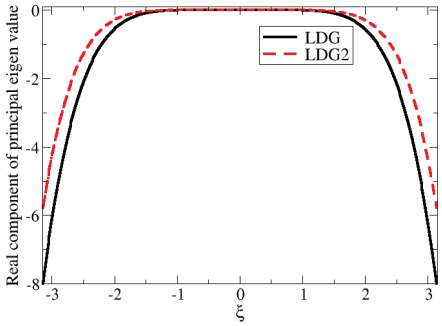

Figure 5: Plot of the real component of the principal eigen value as a function of the non-dimensional frequency for the third order SV.

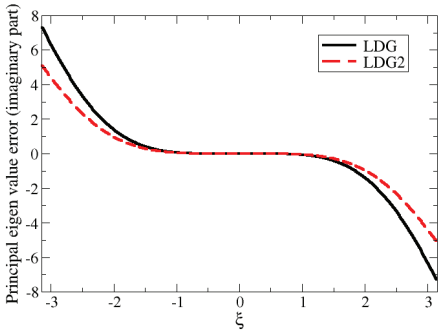

Figure 6: Plot of the error associated with the imaginary component of the principal eigen value as a function of the non-dimensional frequency for the third order SV.

4.3 Fourth order spatial analysis

The fourth order SV of unit length has its interior CV boundaries given by the following local coordinates: $\{0,d,0.5,1-d,1\}$, where d is the length of the first CV in the SV. A value of $d=0.1$ was deemed most accurate in the first paper of this series [17]. This will be used in the remainder of the paper. Fig. 7 shows the variation of the real component of the principal eigen value with respect to the non dimensional frequency ξ for the fourth order SV. The LDG2 formulation generates smaller dissipation error than the LDG formulation. However, it can be seen from Fig. 7(b) that the real component of the principal eigen value of the LDG2 formulation briefly becomes positive. Hence, the scheme is mildly unstable.

In order to remove the instability, a weighted average of the LDG and the LDG2 fluxes is used for the numerical flux. Even a weight of 1.5% for the LDG (i.e., 98.5% for the LDG2) is sufficient to make the scheme stable. This weighted scheme is termed LDG22. Fig. 8 shows the dissipation errors for the LDG and the LDG22 formulations.

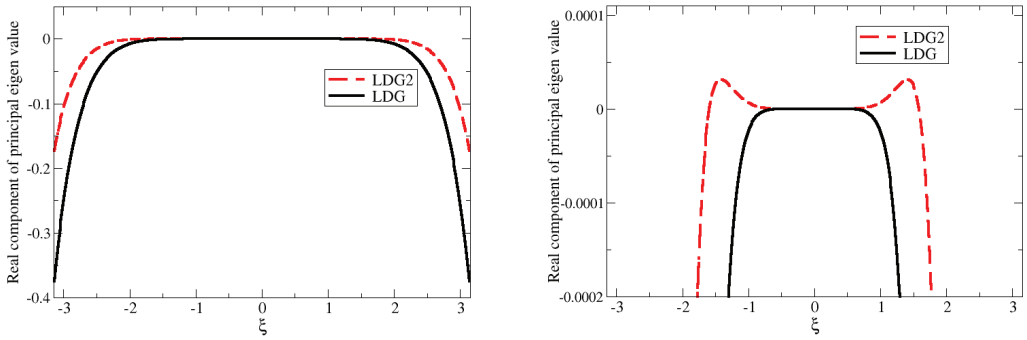

Figure 7: Plot of the real component of the principal eigen value as a function of the non-dimensional frequency for the fourth order SV. Case (a): Across all the wave numbers; Case (b): At small wave numbers.

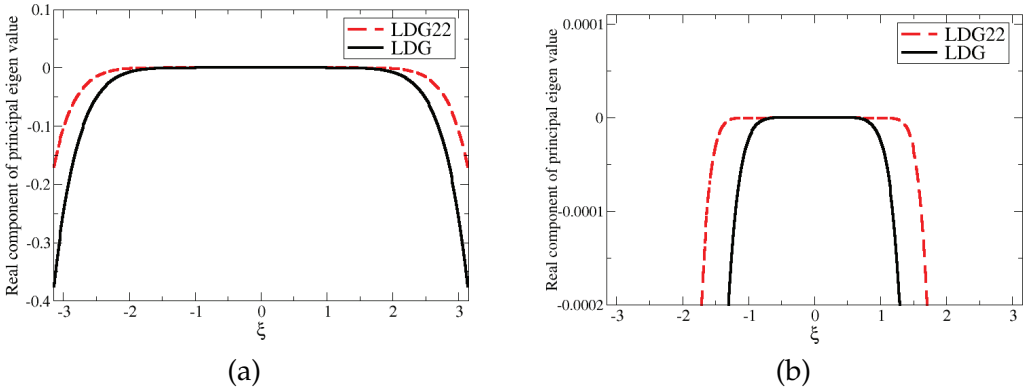

Figure 8: Plot of the real component of the principal eigen value as a function of the non-dimensional frequency for the fourth order SV. Case (a): Across all the wave numbers; Case (b): At small wave numbers.

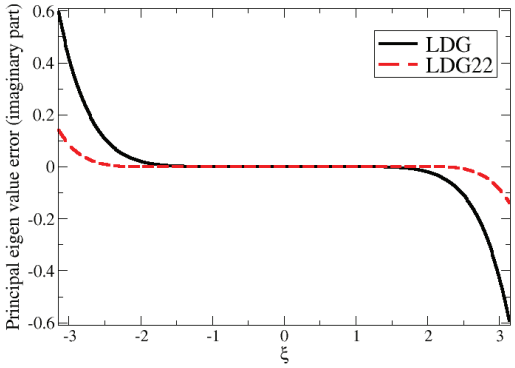

Figure 9: Plot of the error associated with the imaginary component of the principal eigen value as a function of the non-dimensional frequency for the fourth order SV formulation.

Since the LDG22 is predominantly LDG2, their dissipation errors look similar (Fig. 7(a) and Fig. 8(a)). It can also be seen from Fig. 8(b) that the real component of the principal eigen value of the LDG22 formulation is always non-positive. Hence, the LDG22 scheme is stable.

5 Test results

In this section, we provide numerical examples to compare the capabilities of the LDG and the LDG2 (and LDG22) based SV formulations for solving equations containing third spatial derivative terms. A three stage SSP Runge-Kutta scheme was used for time advancement [28]:

$$\overline{u}_i^{(1)} = \overline{u}_i^n - \Delta t R_i(\overline{u}^n), \tag{5.1a}$$

$$\overline{u}_i^{(2)} = \frac{3}{4}\overline{u}_i^n + \frac{1}{4}\left[\overline{u}_i^{(1)} - \Delta t R_i(\overline{u}^{(1)})\right], \tag{5.1b}$$

$$\overline{u}_i^{n+1} = \frac{1}{3}\overline{u}_i^n + \frac{2}{3}\left[\overline{u}_i^{(2)} - \Delta t R_i(\overline{u}^{(2)})\right]. \tag{5.1c}$$

5.1 Test case 1

We compute the solution of the linear equation:

$$u_t + u_{xxx} = 0, \tag{5.2}$$

with an initial condition $u(x,0) = \sin(x)$ and periodic boundary conditions (periodicity $= 2\pi$) over the interval $[0,2\pi]$. This equation has an analytical solution: $u(x,0) = \sin(x+t)$. Both uniform and non-uniform meshes were used in this study. Two types of non-uniform meshes were used. The first type had a recurring pattern of SVs of lengths 0.9Δ

Table 1: $u_t+u_{xxx}=0$. $u_{x,0}=\sin x$. Periodic boundary conditions over interval $[0,2\pi]$. L_2 and L_∞ errors using uniform meshes at $t=1$.

k	Method	Grid	L_2 error	L_2 order	L_∞ error	L_∞ order
1	LDG	10	1.41e-2	-	4.78e-2	-
		20	3.55e-3	1.99	1.27e-2	1.91
		40	8.87e-4	2.00	3.22e-3	1.98
		80	2.22e-4	2.00	8.06e-4	2.00
1	LDG2	10	6.41e-3	-	1.91e-2	-
		20	1.60e-3	2.00	4.88e-3	1.97
		40	4.01e-4	2.00	1.22e-3	2.00
		80	1.00e-4	2.00	3.05e-4	2.00
2	LDG	10	7.31e-4	-	3.31e-3	-
		20	9.26e-5	2.98	4.19e-4	2.98
		40	1.16e-5	2.99	5.31e-5	2.98
		80	1.46e-6	3.00	6.69e-6	2.99
2	LDG2	10	5.22e-4	-	2.21e-3	-
		20	6.57e-5	2.99	2.78e-4	2.99
		40	8.21e-6	3.00	3.50e-5	2.99
		80	1.03e-6	3.00	4.38e-6	3.00
3	LDG	10	2.11e-5	-	1.21e-4	-
		20	1.32e-6	3.99	7.61e-6	3.99
		40	8.30e-8	4.00	4.79e-7	3.99
		80	5.19e-9	4.00	2.99e-8	4.00
3	LDG22	10	1.24e-5	-	6.72e-5	-
		20	7.75e-7	4.00	4.20e-6	4.00
		40	4.84e-8	4.00	2.63e-7	4.00
		80	3.03e-9	4.00	1.64e-8	4.00

Table 2: $u_t+u_{xxx}=0$. $u_{x,0}=\sin x$. Periodic boundary conditions over interval $[0,2\pi]$. L_2 and L_∞ errors using non-uniform (repeating pattern of $0.9\Delta x$ and $1.1\Delta x$) meshes at $t=1$.

k	Method	Grid	L_2 error	L_2 order	L_∞ error	L_∞ order
1	LDG	10	1.60e-2	-	5.83e-2	-
		20	4.08e-3	1.97	1.56e-2	1.90
		40	1.03e-3	1.99	3.96e-3	1.98
		80	2.57e-4	2.00	9.97e-4	1.99
1	LDG2	10	7.24e-3	-	2.43e-2	-
		20	1.82e-3	1.99	6.20e-3	1.97
		40	4.56e-4	2.00	1.56e-3	1.99
		80	1.14e-4	2.00	3.90e-4	2.00
2	LDG	10	8.81e-4	-	4.47e-3	-
		20	1.12e-4	2.97	5.74e-4	2.96
		40	1.41e-5	2.99	7.28e-5	2.98
		80	1.77e-6	3.00	9.16e-6	2.99
2	LDG2	10	6.30e-4	-	3.00e-3	-
		20	7.98e-5	2.98	3.83e-4	2.97
		40	9.98e-6	3.00	4.82e-5	2.99
		80	1.25e-6	3.00	6.02e-6	3.00
3	LDG	10	5.11e-5	-	2.41e-4	-
		20	3.26e-6	3.97	1.55e-5	3.96
		40	2.06e-7	3.98	9.81e-7	3.98
		80	1.30e-8	3.99	6.22e-8	3.98
3	LDG22	10	3.02e-5	-	1.35e-4	-
		20	1.92e-6	3.98	8.53e-6	3.98
		40	1.21e-7	3.99	5.37e-7	3.99
		80	7.54e-9	4.00	3.36e-8	4.00

Table 3: $u_t+u_{xxx}=0$. $u_{x,0}=\sin x$. Periodic boundary conditions over interval $[0,2\pi]$. L_2 and L_∞ errors using non-uniform (repeating pattern of $0.7\Delta x$ and $1.3\Delta x$) meshes at $t=1$.

k	Method	Grid	L_2 error	L_2 order	L_∞ error	L_∞ order
1	LDG	10	2.27e-2	-	7.44e-2	-
		20	5.87e-3	1.95	2.00e-2	1.89
		40	1.49e-3	1.98	5.12e-3	1.97
		80	3.75e-4	1.99	1.29e-3	1.99
1	LDG2	10	1.04e-2	-	3.01e-2	-
		20	2.65e-3	1.97	7.79e-3	1.95
		40	6.68e-4	1.99	1.96e-3	1.99
		80	1.67e-4	2.00	4.90e-4	2.00
2	LDG	10	1.27e-3	-	8.51e-3	-
		20	1.69e-4	2.91	1.16e-3	2.88
		40	2.20e-5	2.94	1.53e-4	2.91
		80	2.79e-6	2.98	1.97e-5	2.96
2	LDG2	10	9.20e-4	-	5.79e-3	-
		20	1.21e-4	2.93	7.76e-4	2.90
		40	1.54e-5	2.97	1.00e-4	2.95
		80	1.93e-6	3.00	1.26e-5	2.99
3	LDG	10	3.98e-4	-	1.31e-3	-
		20	2.62e-5	3.92	8.77e-5	3.90
		40	1.70e-6	3.95	5.71e-6	3.94
		80	1.08e-7	3.98	3.64e-7	3.97
3	LDG22	10	2.37e-4	-	7.37e-4	-
		20	1.54e-5	3.94	4.83e-5	3.93
		40	9.78e-7	3.98	3.10e-6	3.96
		80	6.11e-8	4.00	1.95e-7	3.99

and 1.1Δ, where Δ was the length of the corresponding uniform SV. The second type had a recurring pattern of SVs of lengths 0.7Δ and 1.3Δ. An even number of SVs were used for all the test cases. The L_2 and L_∞ errors and orders of accuracies of the numerical solution at $t=1$ second are given in Tables 1-3. It can be seen that the formulations with k^{th} degree polynomial asymptotically attains $(k+1)^{\text{th}}$ order of accuracy. The LDG2 scheme generates more accurate solutions than the LDG scheme for the 2^{nd} and 3^{rd} order cases. Similarly the LDG22 scheme generates more accurate solutions than the LDG scheme for the 4^{th} order cases. These phenomena are observed for both the uniform and the non-uniform meshes.

5.2 Test case 2

We compute the solution of the non-linear KdV equation [36, 37]:

$$u_t-3(u^2)_x+u_{xxx}=0, \tag{5.3}$$

Table 4: $u_t-3(u^2)_x+u_{xxx}=0$. $u_{x,0}=-2\text{sech}^2(x)$. Domain over the interval $[-10,12]$. Boundary conditions given in Eq. (5.4). L_2 and L_∞ errors using uniform meshes at $t=0.5$.

k	Method	Grid	L_2 error	L_2 order	L_∞ error	L_∞ order
1	LDG	10	2.29e-1	-	1.37e-0	-
		20	7.25e-2	1.66	5.45e-1	1.33
		40	2.08e-2	1.80	1.92e-1	1.50
		80	5.50e-3	1.92	6.05e-2	1.67
		160	1.40e-3	1.97	1.73e-2	1.80
		320	3.51e-4	2.00	4.51e-3	1.94
1	LDG2	10	9.54e-2	-	5.07e-1	-
		20	2.76e-2	1.79	1.73e-1	1.55
		40	7.24e-3	1.93	5.19e-2	1.74
		80	1.85e-3	1.97	1.39e-2	1.90
		160	4.62e-4	2.00	3.45e-3	1.99
		320	1.16e-4	2.00	8.75e-4	2.00
2	LDG	10	8.39e-2	-	7.70e-1	-
		20	1.23e-2	2.77	1.17e-1	2.71
		40	1.83e-3	2.75	2.01e-2	2.55
		80	2.46e-4	2.89	3.29e-3	2.61
		160	3.19e-5	2.95	4.69e-4	2.81
		320	3.99e-6	3.00	5.95e-5	2.98
2	LDG2	10	5.24e-2	-	4.53e-1	-
		20	7.58e-3	2.79	6.69e-2	2.76
		40	1.10e-3	2.78	1.09e-2	2.62
		80	1.46e-4	2.92	1.69e-3	2.69
		160	1.85e-5	2.98	2.29e-4	2.88
		320	2.31e-6	3.00	2.86e-5	3.00
3	LDG	10	2.80e-2	-	2.91e-1	-
		20	2.99e-3	3.23	3.37e-2	3.11
		40	2.81e-4	3.41	3.22e-3	3.39
		80	2.00e-5	3.81	2.94e-4	3.45
		160	1.31e-6	3.93	2.14e-5	3.78
		320	8.27e-8	3.99	1.38e-6	3.96
3	LDG22	10	1.47e-2	-	1.42e-1	-
		20	1.49e-3	3.31	1.51e-2	3.23
		40	1.27e-4	3.55	1.29e-3	3.55
		80	8.32e-6	3.93	1.03e-4	3.65
		160	5.27e-7	3.98	6.85e-6	3.91
		320	3.30e-8	4.00	4.34e-7	3.98

with an initial condition $u(x,0)=-2\text{sech}^2(x)$ over the interval $[-10,12]$. The following boundary conditions were applied:

$$u(-10,t)=g_1(t), \qquad u_x(12,t)=g_2(t), \qquad u_{xx}(12,t)=g_3(t), \tag{5.4}$$

where $g_i(t)$ is obtained from the analytical solution to Eq. (5.3): $u(x,t)=-2\text{sech}^2(x-4t)$. The L_2 and L_∞ errors and orders of accuracies of the numerical solution at $t=0.5$

Table 5: $u_t-3(u^2)_x+u_{xxx}=0$. $u_{x,0}=-2\text{sech}^2(x)$. Domain over the interval $[-10,12]$. Boundary conditions given in Eq. (5.4). L_2 and L_∞ errors using non-uniform (repeating pattern of $0.9\Delta x$ and $1.1\Delta x$) meshes at $t=0.5$.

k	Method	Grid	L_2 error	L_2 order	L_∞ error	L_∞ order
1	LDG	10	2.62e-1	-	1.46e-0	-
		20	8.53e-2	1.62	6.01e-1	1.28
		40	2.50e-2	1.77	2.20e-1	1.45
		80	6.71e-3	1.90	7.11e-2	1.63
		160	1.72e-3	1.96	2.08e-2	1.77
		320	4.31e-4	2.00	5.47e-3	1.93
1	LDG2	10	1.09e-1	-	5.41e-1	-
		20	3.36e-2	1.70	1.99e-1	1.44
		40	9.19e-3	1.87	6.57e-2	1.60
		80	2.41e-3	1.93	1.95e-2	1.75
		160	6.07e-4	1.99	5.17e-3	1.92
		320	1.52e-4	2.00	1.30e-3	1.99
2	LDG	10	1.09e-1	-	1.06e0	-
		20	1.66e-2	2.71	1.65e-1	2.68
		40	2.51e-3	2.73	2.81e-2	2.56
		80	3.43e-4	2.87	4.57e-3	2.62
		160	4.41e-5	2.96	6.51e-4	2.81
		320	5.51e-6	3.00	8.31e-5	2.97
2	LDG2	10	6.86e-2	-	6.27e-1	-
		20	1.03e-2	2.74	9.59e-2	2.71
		40	1.48e-3	2.79	1.54e-2	2.64
		80	1.96e-4	2.92	2.38e-3	2.69
		160	2.48e-5	2.98	3.13e-4	2.93
		320	3.11e-6	3.00	3.93e-5	2.99
3	LDG	10	4.99e-2	-	4.09e-1	-
		20	5.18e-3	3.27	4.83e-2	3.08
		40	4.77e-4	3.44	4.81e-3	3.33
		80	3.45e-5	3.79	4.34e-4	3.47
		160	2.25e-6	3.94	3.20e-5	3.76
		320	1.42e-7	3.98	2.04e-6	3.97
3	LDG22	10	2.64e-2	-	2.06e-1	-
		20	2.57e-3	3.36	2.32e-2	3.15
		40	2.20e-4	3.55	2.13e-3	3.44
		80	1.50e-5	3.87	1.75e-4	3.61
		160	9.51e-7	3.98	1.17e-5	3.90
		320	5.95e-8	4.00	7.38e-7	3.99

second are given in Tables 4-6. It can be seen that a full $(k+1)^{\text{th}}$ order of accuracy is asymptotically attained for the formulations with k^{th} degree polynomial, in spite of the problem being heavily non-linear. Once again, the LDG2 (2^{nd} and 3^{rd} order) and the LDG22 (4^{th} order) schemes generate more accurate solutions than the LDG schemes, for both the uniform and the non-uniform meshes.

Table 6: $u_t-3(u^2)_x+u_{xxx}=0$. $u_{x,0}=-2\text{sech}^2(x)$. Domain over the interval $[-10,12]$. Boundary conditions given in Eq. (5.4). L_2 and L_∞ errors using non-uniform (repeating pattern of $0.7\Delta x$ and $1.3\Delta x$) meshes at $t=0.5$.

k	Method	Grid	L_2 error	L_2 order	L_∞ error	L_∞ order
1	LDG	10	3.21e-1	-	1.82e-0	-
		20	1.14e-1	1.50	7.85e-1	1.21
		40	3.45e-2	1.72	2.97e-1	1.40
		80	9.38e-3	1.88	9.81e-2	1.60
		160	2.43e-3	1.95	2.91e-2	1.75
		320	6.11e-4	1.99	7.71e-3	1.92
1	LDG2	10	1.35e-1	-	6.84e-1	-
		20	4.29e-2	1.66	2.40e-1	1.51
		40	1.20e-2	1.84	7.55e-2	1.67
		80	3.14e-3	1.93	2.15e-2	1.81
		160	7.97e-4	1.98	5.65e-3	1.93
		320	1.99e-4	2.00	1.44e-3	1.97
2	LDG	10	2.45e-1	-	2.61e0	-
		20	3.80e-2	2.69	4.46e-1	2.55
		40	5.70e-3	2.74	7.21e-2	2.63
		80	8.18e-4	2.80	1.18e-2	2.61
		160	1.09e-4	2.90	1.72e-3	2.78
		320	1.39e-5	2.98	2.21e-4	2.96
2	LDG2	10	1.58e-1	-	1.58e0	-
		20	2.42e-2	2.71	2.63e-1	2.59
		40	3.52e-3	2.78	4.07e-2	2.69
		80	4.84e-4	2.86	6.35e-3	2.68
		160	6.36e-5	2.93	8.57e-4	2.89
		320	8.00e-6	2.99	1.09e-4	2.97
3	LDG	10	1.18e-1	-	7.71e-1	-
		20	1.21e-2	3.29	9.71e-2	2.99
		40	1.17e-3	3.37	1.03e-2	3.23
		80	8.73e-5	3.74	9.08e-4	3.51
		160	5.77e-6	3.92	6.75e-5	3.75
		320	3.65e-7	3.98	4.28e-6	3.98
3	LDG22	10	6.38e-2	-	3.95e-1	-
		20	6.30e-3	3.34	4.61e-2	3.10
		40	5.61e-4	3.49	4.46e-3	3.37
		80	3.94e-5	3.83	3.58e-4	3.64
		160	2.53e-6	3.96	2.43e-5	3.88
		320	1.59e-7	3.99	1.53e-6	3.99

5.3 Test case 3

This test case was designed to test the robustness and accuracy of the method for non-linear problems with small coefficient for the third derivative term [36, 37]. We compute the soliton solution of the generic KdV equation:

$$u_t+u_x+\left(\frac{u^4}{4}\right)_x+\varepsilon u_{xxx}=0, \tag{5.5}$$

Table 7: $u_t+u_x+(u^4/4)_x+\varepsilon u_{xxx}=0$. $u_{x,0}=-2\text{sech}^{2/3}(K(x-x_0))$ with $A=0.2275$, $x_0=0.5$, $\varepsilon=2.058e-5$ and $K=3(A^3/40\varepsilon)^{1/2}$. Domain over the interval $[-2,3]$. Boundary conditions given in Eq. (5.7). L_2 and L_∞ errors using uniform meshes at $t=1$.

k	Method	Grid	L_2 error	L_2 order	L_∞ error	L_∞ order
1	LDG	10	4.25e-2	-	3.83e-1	-
		20	1.60e-2	1.41	1.56e-1	1.29
		40	5.39e-3	1.57	6.06e-2	1.37
		80	1.60e-3	1.75	2.15e-2	1.49
		160	4.45e-4	1.85	7.07e-3	1.61
		320	1.13e-4	1.98	2.00e-3	1.82
		640	2.82e-5	2.00	5.11e-4	1.97
1	LDG2	10	2.02e-2	-	1.60e-1	-
		20	7.06e-3	1.52	6.06e-2	1.40
		40	2.30e-3	1.62	2.10e-2	1.53
		80	6.28e-4	1.87	6.64e-3	1.66
		160	1.65e-4	1.93	1.86e-3	1.84
		320	4.15e-5	1.99	4.80e-4	1.95
		640	1.04e-5	2.00	1.21e-4	1.99
2	LDG	10	1.99e-2	-	1.67e-1	-
		20	3.68e-3	2.44	3.37e-2	2.31
		40	7.42e-4	2.31	7.35e-3	2.20
		80	1.39e-4	2.41	1.42e-3	2.37
		160	2.05e-5	2.77	2.49e-4	2.51
		320	2.63e-6	2.96	3.56e-5	2.81
		640	3.31e-7	2.99	4.51e-6	2.98
2	LDG2	10	1.53e-2	-	1.19e-1	-
		20	2.72e-3	2.49	2.33e-2	2.35
		40	5.20e-4	2.39	4.81e-3	2.28
		80	9.06e-5	2.52	8.67e-4	2.47
		160	1.24e-5	2.87	1.40e-4	2.63
		320	1.57e-6	2.98	1.89e-5	2.89
		640	1.96e-7	3.00	2.40e-6	2.98
3	LDG	10	1.66e-2	-	1.46e-1	-
		20	1.93e-3	3.11	2.17e-2	2.77
		40	1.69e-4	3.51	2.69e-3	3.01
		80	1.22e-5	3.79	2.60e-4	3.37
		160	7.90e-7	3.95	1.91e-5	3.77
		320	4.98e-8	3.99	1.27e-6	3.91
		640	3.11e-9	4.00	7.98e-8	3.99
3	LDG22	10	1.04e-2	-	8.59e-2	-
		20	1.11e-3	3.23	1.13e-2	2.93
		40	9.18e-5	3.59	1.22e-3	3.21
		80	6.24e-6	3.88	1.00e-4	3.60
		160	3.95e-7	3.98	7.01e-6	3.84
		320	2.47e-8	4.00	4.51e-7	3.96
		640	1.54e-9	4.00	2.82e-8	4.00

with an initial condition $u(x,0)=A\text{sech}^{2/3}(K(x-x_0))$, with $A=0.2275$, $x_0=0.5$, $\varepsilon=2.058e-5$ and $K=3(A^3/40\varepsilon)^{1/2}$. The analytical solution is

$$u(x,t)=A\text{sech}^{\frac{2}{3}}(K(x-x_0)-\omega t), \tag{5.6}$$

where $\omega=K(1+A^3/10)$.

Table 8: $u_t+u_x+(u^4/4)_x+\varepsilon u_{xxx}=0$. $u_{x,0}=-2\text{sech}^{2/3}(K(x-x_0))$ with $A=0.2275$, $x_0=0.5$, $\varepsilon=2.058e-5$ and $K=3(A^3/40\varepsilon)^{1/2}$. Domain over the interval $[-2,3]$. Boundary conditions given in Eq. (5.7). L_2 and L_∞ errors using non-uniform (repeating pattern of $0.9\Delta x$ and $1.1\Delta x$) meshes at $t=1$.

k	Method	Grid	L_2 error	L_2 order	L_∞ error	L_∞ order
1	LDG	10	4.45e-2	-	4.15e-1	-
		20	1.74e-2	1.35	1.74e-1	1.25
		40	6.17e-3	1.50	6.99e-2	1.32
		80	1.90e-3	1.70	2.56e-2	1.45
		160	5.38e-4	1.82	8.56e-3	1.58
		320	1.38e-4	1.96	2.44e-3	1.81
		640	3.46e-5	2.00	6.23e-4	1.97
1	LDG2	10	2.13e-2	-	1.73e-1	-
		20	8.01e-3	1.41	6.79e-2	1.35
		40	2.66e-3	1.59	2.52e-2	1.43
		80	7.81e-4	1.77	8.42e-3	1.58
		160	2.14e-4	1.87	2.56e-3	1.72
		320	5.41e-5	1.98	6.90e-4	1.89
		640	1.35e-5	2.00	1.74e-4	1.99
2	LDG	10	2.53e-2	-	2.09e-1	-
		20	4.61e-3	2.46	4.32e-2	2.28
		40	9.17e-4	2.33	9.27e-3	2.22
		80	1.77e-4	2.37	1.84e-3	2.33
		160	2.69e-5	2.72	3.32e-4	2.47
		320	3.51e-6	2.94	4.77e-5	2.80
		640	4.45e-7	2.98	6.10e-6	2.97
2	LDG2	10	1.96e-2	-	1.50e-1	-
		20	3.49e-3	2.49	3.00e-2	2.32
		40	6.70e-4	2.38	6.19e-3	2.28
		80	1.24e-4	2.43	1.16e-3	2.42
		160	1.82e-5	2.77	1.91e-4	2.60
		320	2.39e-6	2.93	2.66e-5	2.84
		640	3.01e-7	2.99	3.37e-6	2.98
3	LDG	10	2.09e-2	-	1.85e-1	-
		20	2.57e-3	3.03	2.85e-2	2.70
		40	2.37e-4	3.44	3.64e-3	2.97
		80	1.76e-5	3.75	3.70e-4	3.30
		160	1.18e-6	3.90	2.83e-5	3.71
		320	7.47e-8	3.98	1.92e-6	3.88
		640	4.67e-9	4.00	1.21e-7	3.99
3	LDG22	10	1.31e-2	-	1.09e-1	-
		20	1.54e-3	3.09	1.46e-2	2.90
		40	1.36e-4	3.51	1.59e-3	3.20
		80	9.66e-6	3.81	1.37e-4	3.54
		160	6.29e-7	3.94	9.61e-6	3.83
		320	3.99e-8	3.98	6.26e-7	3.94
		640	2.49e-9	4.00	3.94e-8	3.99

The following boundary conditions were applied over the interval $[-2,3]$:

$$u(-2,t)=g_1(t), \qquad u_x(3,t)=g_2(t), \qquad u_{xx}(3,t)=g_3(t), \tag{5.7}$$

where $g_i(t)$ is obtained from the analytical solution.

The L_2 and L_∞ errors and orders of accuracies of the numerical solution at $t=1$ second are given in Tables 7-9. The findings are identical to that of the above two cases, with the

Table 9: $u_t+u_x+(u^4/4)_x+\varepsilon u_{xxx}=0$. $u_{x,0}=-2\text{sech}^{2/3}(K(x-x_0))$ with $A=0.2275$, $x_0=0.5$, $\varepsilon=2.058e-5$ and $K=3(A^3/40\varepsilon)^{1/2}$. Domain over the interval $[-2,3]$. Boundary conditions given in Eq. (5.7). L_2 and L_∞ errors using non-uniform (repeating pattern of $0.7\Delta x$ and $1.3\Delta x$) meshes at $t=1$.

k	Method	Grid	L_2 error	L_2 order	L_∞ error	L_∞ order
1	LDG	10	4.86e-2	-	5.14e-1	-
		20	2.08e-2	1.22	2.22e-1	1.21
		40	7.97e-3	1.39	9.28e-2	1.26
		80	2.58e-3	1.63	3.52e-2	1.40
		160	7.55e-4	1.77	1.19e-2	1.56
		320	1.98e-4	1.93	3.45e-3	1.79
		640	4.99e-5	1.99	8.87e-4	1.96
1	LDG2	10	2.37e-2	-	2.19e-1	-
		20	9.36e-3	1.34	9.00e-2	1.28
		40	3.22e-3	1.54	3.51e-2	1.36
		80	9.78e-4	1.72	1.22e-2	1.52
		160	2.73e-4	1.84	3.77e-3	1.70
		320	7.02e-5	1.96	1.03e-3	1.87
		640	1.77e-5	1.99	2.63e-4	1.97
2	LDG	10	3.47e-2	-	3.16e-1	-
		20	6.49e-3	2.42	6.42e-2	2.30
		40	1.30e-3	2.32	1.31e-2	2.29
		80	2.63e-4	2.30	2.76e-3	2.25
		160	4.26e-5	2.63	5.16e-4	2.42
		320	5.75e-6	2.89	7.56e-5	2.77
		640	7.49e-7	2.94	1.02e-5	2.89
2	LDG2	10	2.78e-2	-	2.36e-1	-
		20	5.05e-3	2.46	4.72e-2	2.32
		40	9.69e-4	2.38	9.39e-3	2.33
		80	1.84e-4	2.40	1.77e-3	2.41
		160	2.90e-5	2.66	3.10e-4	2.51
		320	3.87e-6	2.91	4.33e-5	2.84
		640	5.00e-7	2.95	5.69e-6	2.93
3	LDG	10	3.18e-2	-	2.94e-1	-
		20	4.12e-3	2.95	4.85e-2	2.60
		40	4.09e-4	3.33	6.50e-3	2.90
		80	3.26e-5	3.65	6.93e-4	3.23
		160	2.26e-6	3.85	5.52e-5	3.65
		320	1.45e-7	3.96	3.80e-6	3.86
		640	9.08e-9	4.00	2.41e-7	3.98
3	LDG22	10	2.05e-2	-	1.78e-1	-
		20	2.51e-3	3.03	2.51e-2	2.83
		40	2.31e-4	3.44	2.82e-3	3.15
		80	1.72e-5	3.75	2.50e-4	3.50
		160	1.14e-6	3.91	1.83e-5	3.77
		320	7.25e-8	3.98	1.23e-6	3.89
		640	4.53e-9	4.00	7.76e-8	3.99

LDG2 (2^{nd} and 3^{rd} order) and the LDG22 (4^{th} order) schemes generating more accurate solutions than the LDG schemes, for both the uniform and the non-uniform meshes On an average, the LDG2 (LDG22 for 4^{th}order) was slower than the LDG, by around 40%, 45% and 50% for the 2^{nd}, 3^{rd} and 4^{th} order simulations respectively.

6 Conclusions

In the present study, we implemented a LDG2 formulation for solving equations containing higher spatial derivative terms in a spectral volume context. A linear Fourier analysis was performed to compare and contrast the dispersion and the dissipation properties of the LDG and the LDG2 formulations. The analysis showed that the LDG2 scheme is stable and generates smaller dissipation and dispersion errors than the LDG formulation for the second and third simulations. The fourth order LDG2 is mildly unstable. However, the instability was removed, by using a weighted average of the LDG and the LDG2 fluxes was used as the numerical flux. Even a weight of 1.5% for the LDG (i.e., 98.5% for the LDG2) was sufficient to ensure stability and yield more accurate solutions than the LDG scheme.

Numerical experiments were conducted to illustrate the accuracy, capability and robustness of this new formulation. Expected orders of accuracy were attained asymptotically for both the linear and the non-linear equations. In addition, the formulation was able to handle stiff convection dominated cases where the coefficients of the third spatial derivative terms are small. As expected, the LDG2 (and the LDG22 for the fourth order) outperforms the LDG scheme for all the orders and all the grids.

Future work will include implicit time discretization procedures, employing penalty based flux formulations (like extensions of the BR2 and the interior penalty schemes), performing Fourier analysis for 2D problems, implementing an implicit p-multigrid algorithm [23] and extending the formulation to equations containing fourth order spatial derivative terms.

The final goal of this research project is to extend the current formulation to handle interactions of non-linear KDV type waves with multiphase flows [2, 4] and turbulent explosions [2–4]. These problems involve the interplay of various complex physical phenomena such as turbulence interaction with solid particles, mixing-induced combustion, shock waves, etc., that were succinctly addressed by Balakrishnan et al. [2–4] using lower order schemes. It would be interesting to assess the performance higher-order schemes for such complex, real-life problems. Efforts along these lines are currently underway and will be addressed in the future.

References

[1] R. Abgrall, On essentially non-oscillatory schemes on unstructured meshes: analysis and implementation, J. Comput. Phys., 114 (1994), 45–58.
[2] K. Balakrishnan and S. Menon, On the role of ambient reactive particles in the mixing and afterburn behind explosive blast waves, Combust. Sci. Tech., 182 (2010), 186–214.
[3] K. Balakrishnan, F. Genin, D. V. Nance and S. Menon, Numerical study of blast characteristics from detonation of homogeneous explosives, Shock Waves, 20(2) (2010), 147–162.
[4] K. Balakrishnan and S. Menon, On turbulent chemical explosions into dilute aluminum particle clouds, Combust. Theor. Model., 14(4) (2010), 583–617.

[5] T. J. Barth and P. O. Frederickson, High-order solution of the Euler equations on unstructured grids using quadratic reconstruction, AIAA Paper No. 90-0013, 1990.
[6] B. Cockburn and C. W. Shu, Runge-Kutta discontinuous Galerkin methods for convection-dominated problems, J. Sci. Comput., 16(3) (2001), 173–261.
[7] B. Cockburn and C.-W. Shu, The local discontinuous Galerkin method for time-dependent convection diffusion system, SIAM J. Numer. Anal., 35 (1998), 2440–2463.
[8] M. Delanaye and Y. Liu, Quadratic reconstruction finite volume schemes on 3D arbitrary unstructured polyhedral grids, AIAA Paper No. 99-3259-CP, 1999.
[9] R. Harris, Z. J. Wang and Y. Liu, Efficient quadrature-free high-order spectral volume method on unstructured grids: theory and 2D implementation, J. Comput. Phys., 227 (2008), 1620–1642.
[10] R. Harris and Z. J. Wang, High-order adaptive quadrature-free spectral volume method on unstructured grids, Comput. Fluids, 38 (2009), 2006–2025.
[11] A. Harten, B. Engquist, S. Osher and S. Chakravarthy, Uniformly high order essentially non-oscillatory schemes III, J. Comput. Phys., 71 (1987), 231.
[12] R. Kannan, High order spectral volume method for moment models in semiconductor device simulations: formulation in 1D and application to a p-multigrid method, Int. J. Numer. Methods Biom. Eng., 27(9) (2011), 1362–1375.
[13] R. Kannan, High order spectral volume method for moment models in semiconductor device simulations II: accuracy studies and performance enhancements using the penalty and the BR2 formulations, Int. J. Numer. Methods Biom. Eng., 27(5) (2011), 650–665.
[14] R. Kannan and Z. J. Wang, A study of viscous flux formulations for a p-multigrid spectral volume Navier stokes solver, J. Sci. Comput., 41(2) (2009), 165–199.
[15] R. Kannan and Z. J. Wang, LDG2: A variant of the LDG viscous flux formulation for the spectral volume method, J. Sci. Comput., 46(2) (2011), 314–328.
[16] R. Kannan and Z. J. Wang, The direct discontinuous Galerkin (DDG) viscous flux scheme for the high order spectral volume method, Compute. Fluids, 39(10) (2010), 2007–2021.
[17] R. Kannan, A high order spectral volume formulation for solving equations containing higher spatial derivative terms: formulation and analysis for third derivative spatial terms using the LDG discretization procedure, Commun. Comput. Phys., 10(5) (2011), 1257–1279.
[18] R. Kannan and Z. J. Wang, Curvature and entropy based wall boundary condition for the high order spectral volume Euler solver, Comput. Fluids, 44(1) (2011), 79–88.
[19] R. Kannan, A high order spectral volume method for elastohydrodynamic lubrication problems: formulation and application of an implicit p-multigrid algorithm for line contact problems, Comput. Fluids, 48(1) (2011), 44–53.
[20] R. Kannan and Z. J. Wang, A high order spectral volume solution to the Burgers' equation using the Hopf-Cole transformation, Int. J. Numer. Methods Fluids, DOI: 10.1002/fld.2612.
[21] R. Kannan and Z. J. Wang, Improving the high order spectral volume formulation using a diffusion regulator, Commun. Comput. Phys., 12 (2012), 247–260.
[22] R. Kannan, High Order Spectral Volume and Spectral Difference Methods on Unstructured Grids, Thesis (Ph.D.)-Iowa State University, 2008, Publication Number: AAI3342262; ISBN: 9780549997177; Source: Dissertation Abstracts International, 70-01, 0437.
[23] C. Liang, R. Kannan and Z. J. Wang, A p-multigrid spectral difference method with explicit and implicit smoothers on unstructured grids, Comput. Fluids, 38(2) (2009), 254–265.
[24] M.-S.Liou and C. Steffen, A new flux splitting scheme, J. Comput. Phys., 107 (1993), 23–39.
[25] Y. Liu, M. Vinokur and Z. J. Wang, Spectral (finite) volume method for conservation laws on unstructured grids V: extension to three-dimensional systems, J. Comput. Phys., 212 (2006),

454–472.
[26] P. L. Roe, Approximate Riemann solvers, parameter vectors and difference schemes, J. Comput. Phys., 43 (1981), 357–372.
[27] V. V. Rusanov, Calculation of interaction of non-steady shock waves with obstacles, J. Comput. Math. Phys., 1 (1961), 267–279.
[28] C-W. Shu, Total-variation-diminishing time discretizations, SIAM J. Sci. Stat. Comput., 9 (1988), 1073–1084.
[29] Y. Sun, Z. J. Wang and Y. Liu, Spectral (finite) volume method for conservation laws on unstructured grids VI: extension to viscous flow, J. Comput. Phys., 215 (2006), 41–58.
[30] K. Van den Abeele, T. Broeckhoven and C. Lacor, Dispersion and dissipation properties of the 1D spectral volume method and application to a p-multigrid algorithm, J. Comput. Phys., 224(2) (2007), 616–636.
[31] Z. J. Wang, Spectral (finite) volume method for conservation laws on unstructured grids: basic formulation, J. Comput. Phys., 178 (2002), 210.
[32] Z. J. Wang and Y. Liu, Spectral (finite) volume method for conservation laws on unstructured grids II: extension to two-dimensional scalar equation, J. Comput. Phys., 179 (2002), 665.
[33] Z. J. Wang and Y. Liu, Spectral (finite) volume method for conservation laws on unstructured grids III: extension to one-dimensional systems, J. Sci. Comput., 20 (2004), 137.
[34] Z. J. Wang and Y. Liu, Spectral (finite) volume method for conservation laws on unstructured grids IV: extension to two-dimensional Euler equations, J. Comput. Phys., 194 (2004), 716.
[35] Z. J. Wang and Y. Liu, Extension of the spectral volume method to high-order boundary representation, J. Comput. Phys., 211 (2006), 154–178.
[36] J. Yan and C.-W. Shu, A local discontinuous Galerkin method for KdV type equations, SIAM J. Numer. Anal., 40(2) (2002), 769–791.
[37] J. Yan and H. Liu, A local discontinuous Galerkin method for the Korteweg-de Vries equation with boundary effect, J. Comput. Phys., 215 (2006), 197–218.
[38] M. Zhang and C. W. Shu, An analysis of three different formulations of the discontinuous Galerkin method for diffusion equations, Math. Models Methods Appl. Sci., 13 (2003), 395–413.